Journal of Alloys and Compounds, Volume 1004, November 2024, Article number 175902
DOI:10.1016/j.jallcom.2024.175902

Flexible, scalable hierarchical graphene foam decorated with nickel layer for highly sensitive enzyme-free glucose sensing

Xiaodong Ji [a,b], Huihui Jin [c,d,*], Wei Qian [d], Zhe Wang [e], Zixin Zhang [b], Zhugen Yang [f], Daping He [a,b,d,*]

[a] Sanya Science and Education Innovation Park of Wuhan University of Technology, Sanya 572000, China

[b] School of Materials Science and Engineering, Wuhan University of Technology, Wuhan 430070, China

[c] School of Science, Wuhan University of Technology, Wuhan 430070, China

[d] Hubei Engineering Research Center of RF-Microwave Technology and Application, Wuhan University of Technology, Wuhan 430070, China

[e] State Key Laboratory of Advanced Technology for Materials Synthesis and Processing, Wuhan University of Technology, Wuhan 430070, China

[f] School of Water, Energy and Environment, Cranfield University, Cranfield, MK43 0AL, United Kingdom

[*]Corresponding author.

Email-address: jinhuihui@whut.edu.cn (Huihui Jin), hedaping@whut.edu.cn (Daping He)

Published by Elsevier. This is the Author Accepted Manuscript issued with: Creative Commons Attribution License (CC:BY 4.0).
The final published version (version of record) is available online at DOI:10.1016/j.jallcom.2024.175902. Please refer to any applicable publisher terms of use.

Abstract

Developing functional electrode materials for enzyme-free glucose electrochemical sensing is indispensable and challenging for rapid detection and instant diagnosis. Optimizing the microstructure of electrodes to enhance molecule accessibility, facilitate rapid mass transfer, and enlarge electrochemical active surface area is critical prerequisite for improving the electrochemical analytical performance. Herein, we develop a flexible graphene foam electrode with high conductivity and multilayer channel structure achieving efficient enzyme-free glucose sensor through one-step electrodeposition of nickel. The almost defect-free graphitic structure and layered multi-channel configuration enable the graphene foam to exhibit high conductivity, large specific surface area, and excellent mechanical performance. These properties result in efficient electron transmission and mass transfer, enabling the graphene foam to function as an excellent electrode substrate material in electrochemical sensors. Thus, the detecting electrode (Ni/GF) produced by electrodepositing nickel on graphene foam, demonstrates elevated sensitivity (1719.4 μA mM^{-1} cm^{-2}), low limit of detection (0.2 μM), exceptional stability, and excellent flexibility for glucose detection. More importantly, the prepared electrode has been successfully applied to artificial sweat and tea, indicating its practical utility. The attractive analytical outcomes suggest that our layered multi-channel graphene foam has the potential to serve as a crucial foundational working electrode for designing efficient electrochemical sensor.

Keywords: graphene foam, nickel, enzyme-free, glucose electrochemical sensing

1. Introduction

The electrode serves as direct reaction interfaces and plays a significant role in sensing performance such as sensitivity, limits of detection, stability, and response time [1–3]. At present, glassy carbon electrodes have been widely applied in electrochemical sensing as commercial electrodes [4–7]. Unfortunately, the low specific surface area, inferior electrical conductivity, poor stability, sluggish electrochemical kinetics, and limited flexibility of these electrode materials hinder the development and implementation of sensors, thus there is an urgent need for the development of new materials for electrodes [8–10].

In the past few decades, numerous efficient and sophisticated two-dimensional (2D) and three-dimensional (3D) electrochemical sensing electrodes have been produced, such as screen-printed carbon electrodes, carbon paper (CP), and nickel foam [11–16]. Compared to 2D structured electrodes, engineering 3D structural configurations with interconnected channels can offer a stable confinement effect and encourage a more comprehensive contact between the electrode and the electrolyte, hence enhancing electrode stability and mass transport [17–21]. Recently, Farid et al. used nickel foam as an electrode substrate material to prepare a robust carbon nanocoils/nickel foam scaffold by chemical vapor deposition for enzyme-free glucose sensing [22]. Nickel foam possesses an ideal 3D porous structure, high electrical conductivity, and a significant specific surface area, making it extensively applicable as a working electrode. However, nickel foam is too stiff to flexible wearable sensors. To this end,

carbon paper is favored because of its excellent properties. Yan et al. prepared glucose oxidase-modified three-dimensional gold/CP electrode for electrochemical sensing of glucose [23]. However, the low electrical conductivity of carbon paper substrates restricts electron transfer, thereby compromising the analytical performance for glucose detection. Graphene is a promising electrochemical material for direct electrochemical sensing due to its high carrier mobility, excellent mechanical properties, large specific surface area, and excellent biocompatibility [24–26]. Lou et al. prepared a 3D porous laser-induced graphene (LIG) electrode based on polyether sulfone membrane and developed an enzyme-free glucose sensor with electrodepositing gold nanoparticles onto the working electrode [27]. While LIG offers numerous active sites, efficient diffusion pathways, and excellent structural flexibility, its development in the sensing field is hindered by short lifespan and poor precursor uniformity [28]. Therefore, it is great significance to optimize the design and characteristics of graphene-based electrodes to enhancing overall sensing capabilities.

Here, we present a nickel-decorated flexible electrode built on high conductivity (2.58×10^4 S m^{-1}), layered multi-channel structure of graphene foam substrate for efficient enzyme-free electrochemical glucose sensing. The graphene foam is obtained by high-temperature reduction at 2850 ℃. The high degree of graphitization results to high conductivity. Simultaneously, gas release during the reduction process creates a multilayer channel structure. These properties enable efficient electron transfer and a large specific surface area for reactions, suitable for use directly or in combination with

other compounds as electrodes for wearable electrochemical sensors. Thus, the prepared nickel-decorated graphene foam electrode (Ni/GF) inherits a multi-channel hierarchical 3D configuration, greatly increasing the abundance of active sites on the electrode and enhancing efficient electron transfer. Consequently, the Ni/GF electrode exhibits wide linear range (0.5 μM–1 mM), high sensitivity (1719.4 μA mM^{-1} cm^{-2}), rapid response time (3 s), low limit of detection (LOD) (0.2 μM), excellent flexibility, and favorable anti-interference ability. The feasibility of the developed Ni/GF electrodes for practical applications was assessed using artificial sweat and tea samples, demonstrating consistent and reliable performance. This work provides promising strategies for future development of ultrasensitive sensors and point-of-care electrochemical analytical devices.

2. Experimental

2.1 Reagents

Graphene oxide (GO) was purchased from Wuxi Chengyi Education Technology Co., Ltd (China). Nickel (II) sulfate hexahydrate ($NiSO_4 \cdot 6H_2O$), ascorbic acid (AA), dopamine (DA), sucrose (Suc), aspartic acid (Asp), nickel (II) chloride hexahydrate ($NiCl_2 \cdot 6H_2O$), glucose, fructose (Fu), lactose (Lac), boric acid (H_3BO_3), uric acid (UA), sodium hydroxide (NaOH) and sodium chloride (NaCl) were obtained from Shanghai Macklin Biochemical Technology Co., Ltd (China). The artificial sweat solution was purchased from Beijing Bio-Tech Co., Ltd (China). Tea was bought from a local shop

in Wuhan (China).

2.2 Preparation of GF

The graphene foam was developed via high-temperature thermal reduction using graphene oxide (GO) as the precursor. Briefly, GO was dissolved in deionized water at a mass ratio of 1: 66. The GO dispersion was uniformly stirred using a homogenizer, followed by coating the stirred GO dispersion on polyethylene terephthalate film to form a GO film. Subsequently, the GO film underwent heating at 1300 ℃ for 2 h and then at 2850 ℃ for 1 h in an argon atmosphere to obtain the graphene foam (GF). Compressing graphene foam (cGF) was achieved by applying a pressure of 200 MPa to the GF.

2.3 Preparation of Ni/GF

The Ni/GF was developed by a simple one-step electrodeposition process. Prior to the modification, the GF was repeatedly rinsed with ethanol and deionized (DI) water, followed by drying under vacuum. Nickel was electrodeposited onto the GF using a two-electrode direct current (DC) power supply, with a graphite rod serving as the anode. The GF was electrodeposited at 0.2 A cm^{-2} for 30 s in an electrolyte containing 2.3 M $NiSO_4 \cdot 6H_2O$, 0.1 M $NiCl_2 \cdot 6H_2O$, and 0.3 M H_3BO_3. The obtained Ni/GF was washed with DI water. Ni/cGF was prepared using the identical procedure as described above for comparison.

2.4 Electrochemical measurement

All electrochemical tests were conducted using Autolab PGSTAT302N workstation (Metrohm, Switzerland). The working electrode (WE) is the Ni/GF or the bare GF, a Pt flake served as the counter electrode (CE), and an Ag/AgCl electrode served as the reference electrode (RE). The electrochemical performance of glucose on the electrode was investigated using cyclic voltammetry (CV) in range of 0-0.8 V with the scan rate of 50 mV s^{-1} unless otherwise stated. Amperometric i-t curves were performed under constant magnetic stirring. All electrochemical measurements were conducted in 0.1 M NaOH aqueous solution. In all experiments the reaction area of working electrodes was maintained at 1 × 1 cm^2.

3. Results and discussion

3.1 Morphological and structural characterization

The preparation process of the Ni/GF is schematically depicted in Fig. 1a. Initially, graphene foam was fabricated via blade coating and then heat-treated at various temperatures. As the temperature increased, oxygen-containing functional groups on graphene oxide decomposed into gas, leading to the formation of multi-layered channel structures. Subsequently, the defect structure of graphene was gradually repaired, which is conducive to electron transfer, making the GF exhibit high conductivity (2.58×10^4 S m^{-1}). Finally, nickel particles were uniformly deposited on the GF surface and interlayer via one-step electrodeposition. The morphology of bare and modified GF was

analyzed using scanning electron microscopy (SEM). The surface of bare GF exhibits a significant number of micro wrinkles (Fig. 1b), which providing a large specific surface area for electrodeposition. Fig. 1c shows a nickel layer that has been deposited on the GF surface, formed by closely connected particles. Then, optical profilometry was employed to measure the surface roughness of Ni/GF (Ra = 4.382 μm), revealing its surface roughness features (Fig. 1d). As a control, tightly stacked graphene foam was prepared by compressing GF (cGF). As shown in Fig 1e, the surface of the cGF appears relatively flat with fewer wrinkles, resulting in a largely flat deposition of nickel on its surface. The surface morphology in Fig. 1f and roughness test in Fig. 1g of Ni/cGF (Ra = 1.183 μm) provide evidence for this. Notably, the rougher nickel layer on GF surface is beneficial for providing more reaction area and promoting reaction progress.

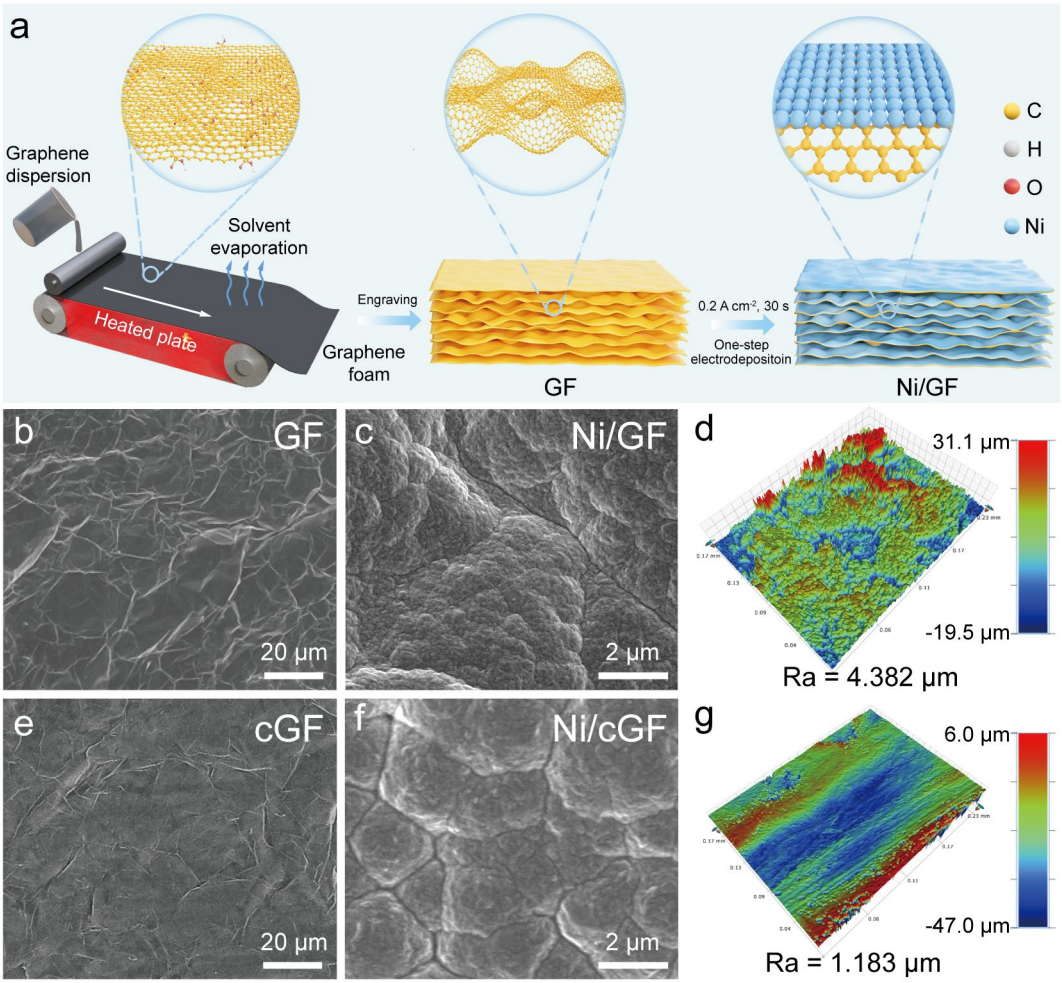

Fig. 1. (a) Schematic diagram of the preparation of the Ni/GF. (b) Top view of the GF and (c) Ni/GF. (d) Top surface height profile images of Ni/GF taken by optical profilometry. (e) Top view of the cGF and (f) Ni/cGF. (g) Top surface height profile images of Ni/cGF taken by optical profilometry.

In cross-sectional SEM image, the bare GF formed by multilayer graphene exhibits a multi-channel wrinkled layered structure (Fig. 2a). The layered multi-channel structure inside the GF was observed through three-dimensional CT. Fig. S1 displays the three-dimensional morphology inside the GF, revealing numerous connected pores. These structural characteristics of GF are conducive to the deep internal growth of Ni. As shown in Fig. 2b, Ni fully grows within the inner layer of GF, and the resulting

electrode preserves its original multilayer structure, which enhances the accessibility of the electrolyte to the electrode material and promotes efficient charge transfer to improve overall electrochemical performance. Fig. 2b presents the spatial distribution of C and Ni elements throughout the layered multi-channel structure, as demonstrated by energy dispersive X-ray spectroscopy (EDS) mapping. Inversely, the cross-sectional SEM image and elemental mapping of the cGF (Fig. S2) show a densely stacked layered structure, in which nickel was only deposited on surface of cGF. Fig. 2c illustrates the good flexibility of the Ni/GF electrode, suggesting its potential for wearable devices. Besides, a straightforward adhesion test was conducted in comparison with Ni/cGF to reflect the structural integrity of the Ni/GF electrode (Fig. 2d). The finding manifests that the Ni layer on GF is difficulty to remove (Fig. 2e-f). The tight contact between the Ni layer and the GF substrate facilitates electron transmission throughout the electrochemical reaction.

Further in the materials characterization, the Raman spectra of the prepared GF exhibit a minimal D peak at 1348.3 cm^{-1} and a prominent G peak at 1580.2 cm^{-1} (Fig. 2g). The low I_D/I_G value (0.032) indicates that GF exhibits a high degree of graphitization. In addition, the asymmetric 2D peak was fitted to reveal peaks at $2D_1$ (2669.3 cm^{-1}) and $2D_2$ (2720.4 cm^{-1}) for AB stacking, alongside $2D_T$ (2701.5 cm^{-1}) for turbostratic stacking (Fig. S3). GF shows a noticeably high AB stacking degree, indicating that graphitization facilitated carbon atomic rearrangement, resulting in the formation of high-quality graphite microcrystals [29,30]. Additionally, the XRD pattern

of GF comprises two sharp characteristic peaks of C (002) located at 26.5° and C (004) located at 54.8° (Fig. 2h). These observations indicate that the GF has a limited number of lattice defects and possesses a highly sp^2 hybridized carbon atom structure after high-temperature reduction [31,32]. From the XRD pattern of Ni/GF, the diffraction peak of carbon remains unchanged, suggesting that the graphitized structure of GF is not destroyed by electrodeposition process. Additionally, there are three diffraction peaks at 44.8°, 52.2°, and 76.6°, corresponding to the (111), (200), and (220) facets of the Ni crystal, respectively [33]. Subsequently, the surface elemental composition and chemical valence of Ni/GF were analyzed and determined by XPS. The XPS spectra confirm the presence of C, O, and Ni elements in the Ni/GF (Fig. S4). Fig. S5 displays the high-resolution spectrum of C 1s, revealing fitting peaks at 284.77 eV, 285.65 eV, and 288.49 eV, representing the C-C/C=C, C-O, and C=O bonds, respectively. The low C-O/C=O ratio implies a high degree of reduction in the GF, which corroborates the previous Raman and XRD results. In Fig. 2i, the peak of Ni 2p at 852.9 eV and 869.8 eV are indicative of metallic Ni, consistent with the earlier XRD result. Besides, two prominent peaks corresponding to Ni $2p_{3/2}$ at 856.4 eV (or 858.0 eV) and Ni $2p_{1/2}$ at 873.9 eV (or 875.6 eV) were observed, indicating the oxidized species of $Ni^{2+/3+}$ [34–36]. O 1s spectrum in Fig. S6 presents two asymmetric peaks at 531.76 eV and 532.25 eV, corresponding to $O_{Lattice}$ and $O_{Adsorbed}$, respectively. The presence of $O_{Lattice}$ and the oxidized state of Ni suggest the inevitably formation of NiOx species on the Ni/GF surface [37]. Additionally, the water contact angle of Ni/GF (76.99°) was smaller than

that of GF (90.00°) (Fig. S7), suggesting that the Ni oxide layer enhances hydrophilicity and facilitates improved contact between Ni/GF and the electrolyte.

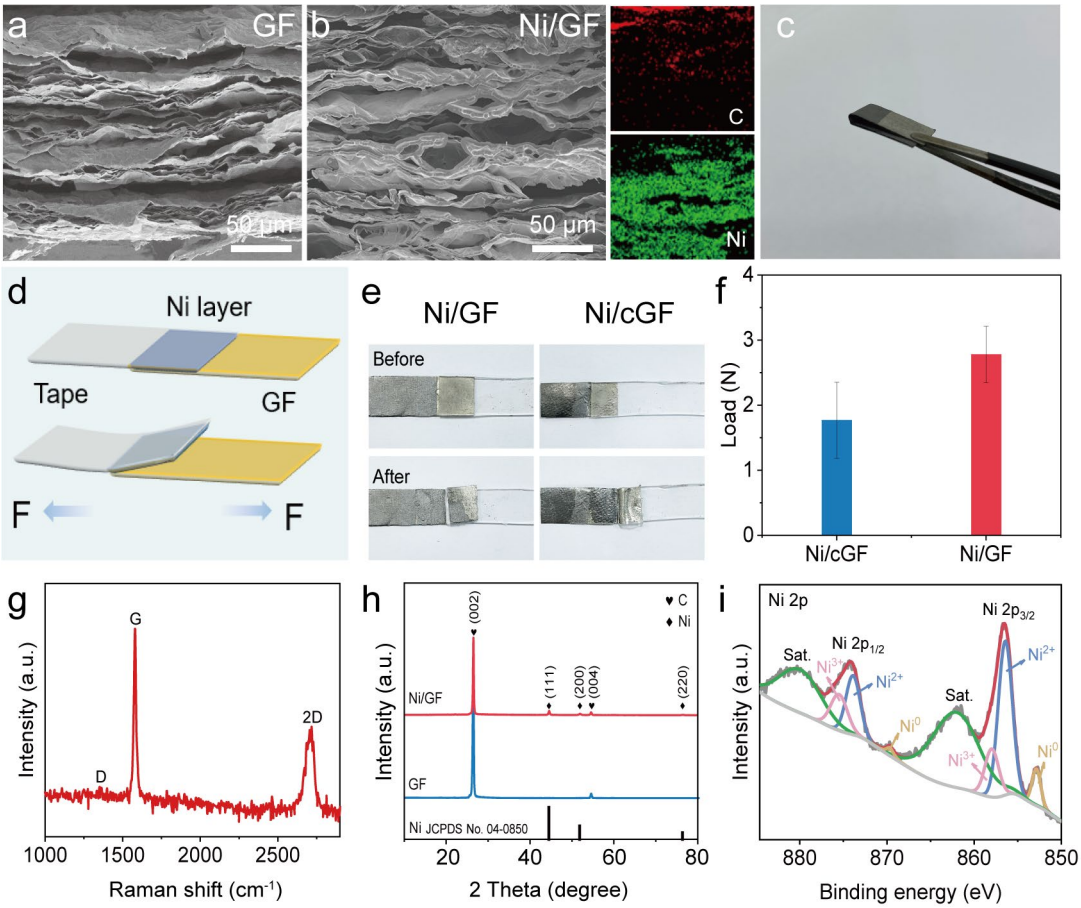

Fig. 2. (a) Cross-sectional morphology of GF. (b) Cross-sectional morphology of Ni/GF and corresponding EDS mapping. (c) Digital photograph of the prepared Ni/GF, exhibiting excellent flexibility. (d) Schematic diagram of adhesion testing between coating and substrate. (e) Digital photographs before and after stretching. (f) Bar diagram of the adhesion of coatings on different substrates. (g) Raman spectrum of GF. (h) X-ray diffraction pattern of the GF and Ni/GF. (i) High-resolution Ni 2p XPS spectrum of Ni/GF.

3.2 Electrochemical sensing for glucose detection

To evaluate the applicability of Ni/GF in electrochemical sensing, the performance of Ni/GF for detecting the small biomolecule glucose was tested. Fig. 3a displays the CVs of the bare GF, Ni/cGF, and Ni/GF under a scan rate of 50 mV s^{-1}, both in the absence and presence glucose of 1 mM. The CV of bare GF exhibits no discernible current density peak, and remains virtually unchanged with the addition of glucose, indicating that the electrochemical oxidation reaction of bare GF to glucose is inactive. On the contrary, both Ni/cGF and Ni/GF exhibit noticeable redox peak without glucose, which can be attributed to the redox reaction of Ni (II)/Ni (III) under alkaline conditions. More importantly, the addition of 1 mM glucose resulted in a significant increase in the oxidation peak current density, which was about 1.9 times higher for Ni/GF than for Ni/cGF (Fig. 3b). Then, we also conducted comparative tests using commercial carbon paper. In both the presence or absence of glucose, Ni/GF consistently shows a higher current density response, which can be attributed to the high conductivity of GF compared to commercial carbon paper (Fig. S8). This enhanced conductivity facilitates efficient and rapid electron transfer. Moreover, the electrochemical impedance spectroscopy (EIS) results show that the Ni/GF electrode exhibits minimum charge transfer resistance (Fig. 3c). The lower R_{ct} value signifies enhanced electrochemical kinetics, promoting faster electron transfer at the Ni/GF electrode. These findings further supporting its favorable electrochemical performance and validating the results obtained from CV.

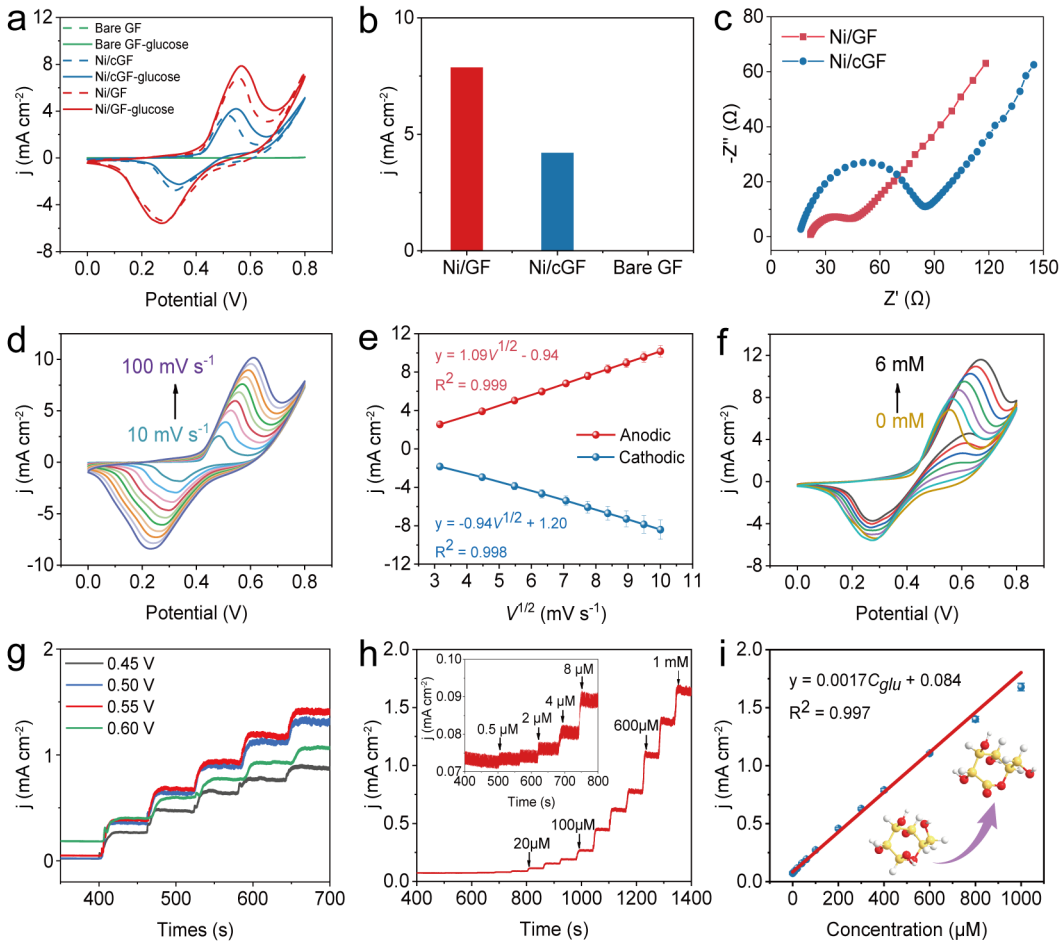

Fig. 3. (a) CVs of bare GF, Ni/cGF, and Ni/GF in the absence or presence glucose. (b) Histogram of oxidation peak current density of bare GF, Ni/cGF, and Ni/GF. (c) EIS results comparing Ni/GF and Ni/cGF. (d) CVs of the Ni/GF at different scan rates. (e) Plot of peak current density against the square root of the scan rate for Ni/GF. (f) CVs of Ni/GF with varying concentrations of glucose. (g) Amperometric responses of Ni/GF at distinct working potentials. (h) Amperometric responses of Ni/GF with successive injection of glucose (0.5 μM–1 mM) at 0.55 V (inset: enlarged plot in the range from 400 to 800 s). (i) Linear curve peak of current density versus glucose concentrations for Ni/GF.

We then performed CV tests at different scanning rates (10-100 mV s^{-1}) in a solution

of 0.1 M NaOH and 1 mM glucose to gain insight into the kinetic properties of glucose reactions on the active surface area of the Ni/GF electrode. As shown in Fig. 3d, the anode and cathode peak current (I_{pa} and I_{pc}) density gradually increase with the scanning rate. Furthermore, the shifts of the anode and cathode peak potentials (E_{pa} and E_{pc}) towards more positive and negative values, respectively, indicates a quasi-reversible redox mechanism of the process. It was found that the magnitude of the current response is linear with the square root of the scanning rate (Fig. 3e). The linear regression equations are I_{pa} (mA) = $1.09v^{1/2} - 0.94$ ($R^2 = 0.999$) and I_{pc} (mA) = $-0.94v^{1/2} + 1.20$ ($R^2 = 0.998$), suggesting that electrooxidation of glucose at the Ni/GF electrode is controlled by a diffusion mechanism. The glucose adsorbed on the Ni/GF electrode surface can be quantified using the Brown-Anson model [38]:

$$I_p = nFAQv/4RT = n^2F^2Av\Gamma/4RT \quad (1)$$

As a result, the adsorption of glucose on the Ni/GF electrode surface was determined to be 1.45×10^{-7} mol cm^{-2}.

Additionally, the CV responses of the Ni/GF electrode on different glucose concentration in the electrolytes were also evaluated. As can be seen from Fig. 3f, with the continuous increase of glucose concentration from 0 to 6 mM, the peak oxidation current density increases significantly and shows a linear relationship ($R^2 = 0.995$) (Fig. S9). These results suggest that Ni/GF electrodes exhibit excellent catalytic performance for glucose detection over a wide concentration range.

The sensitivity and detection limit of the Ni/GF electrode for glucose detection were

evaluated using amperometric methods. The optimal potential for oxidizing glucose was first studied. As presented in Fig. 3g, with the continuous addition of 200 μM glucose, the response current density reaches steady state faster at 0.55 V. The scatter plot (Fig. S10) at different voltages shows the largest slope at 0.55 V, indicating enhanced sensitivity. Hence, 0.55 V was determined to be the most appropriate working potential for subsequent tests. Fig. 3h displays a stable amperogram for Ni/GF electrode, the current density response gradually increased with the addition of different concentrations of glucose (0.5 μM–1 mM), and the electrode exhibited a significant response even with the addition of very low concentrations of glucose. Fig. S11 shows that the Ni/GF electrode takes only 3 s to stabilize when transitioning between different glucose concentrations. This rapid response reflects efficient electron transfer during glucose oxidation, demonstrating the excellent performance of the developed electrode in glucose detection. Specifically, the layered multi-channel structure of Ni/GF enhances the electrochemical active surface area and provides wide ion channels, allowing a large number of active sites to interact with the target molecule. Glucose undergoes rapid adsorption, diffusion, and electrooxidized to gluconolactone, significantly enhancing the oxidation current density response. Fig. 3i shows the calibration curve of the steady-state current density response plotted against glucose concentration, demonstrating excellent linearity. The regression equation derived from the relationship between glucose concentration and oxidation current density is expressed as j (mA cm^{-2}) = 0.0017C_{glu} (μM) + 0.084 (R^2 = 0.997). The sensitivity of the

Ni/GF electrode is 1719.4 μA mM^{-1} cm^{-2}. According to the equation: LOD = 3σ/S, the LOD of the Ni/GF electrode was worked out to be 0.2 μM (S/N = 3), which is superior to most currently reported enzyme-free glucose sensing electrodes (Table S1).

High sensitivity and selectivity are essential for the developed sensors, as there is always interference from various substances when detecting glucose. We evaluated the specificity of the developed sensors to validate the practical application of the Ni/GF electrode. Although the concentrations of other organic and inorganic interferents are significantly lower than that of glucose, these interferents can adversely affect glucose detection [39–42]. To examine the selective electrochemical response of the Ni/GF sensor to glucose molecules, a preferred ratio of 10: 1 (glucose to interferents) was utilized in the subsequent testing. Fig. 4a presents the amperometric response of 1 mM glucose and 0.1 mM of multiple interfering substances, such as sucrose (Suc), ascorbic acid (AA), uric acid (UA), fructose (Fru), aspartic acid (Asp), lactose (Lac), and NaCl, sequentially injected into 0.1 M NaOH electrolyte. Ni/GF sensors exhibit a weak current density response to interferents, and their addition does not affect the electrode's apparent response current density to glucose. This is attributed to the fact that interferents are not easily electrochemically oxidized in an alkaline medium [33]. The histogram presented in Fig. 4b shows the change in current density for glucose and interferents, clearly demonstrating that the developed Ni/GF electrode is significantly selective toward glucose. Fig. 4c displays the current density response during continuous testing for 10000 s after the addition of glucose. After the addition of

glucose, there is a rapid increase in current density, and the electrical signal remains relatively stable without a significant decline over the course of the testing period. However, the current density response of Ni/cGF shows a significant decreasing trend during continuous testing for 10000 s (Fig. S12), which could be due to the weak bonding force between nickel particles and cGF, leading to a decrease in catalyst stability. Furthermore, the Ni/GF electrode retains approximately 96.5% of the original current density after one week of continuous testing (Fig. 4d), confirming its favorable long-term stability. Additionally, to study the reproducibility of the prepared electrodes, six electrodes were prepared using the same method for testing. Fig. 4e shows that the peak current density of 1 mM glucose with different electrodes is quite similar, the relative standard deviation is calculated as 2.36%, suggesting that the Ni/GF electrode possesses excellent reproducibility. Moreover, the electrochemical properties of the prepared electrode barely changed after bending at 90° (Fig. 4f), demonstrating the exceptional flexibility of the Ni/GF electrode.

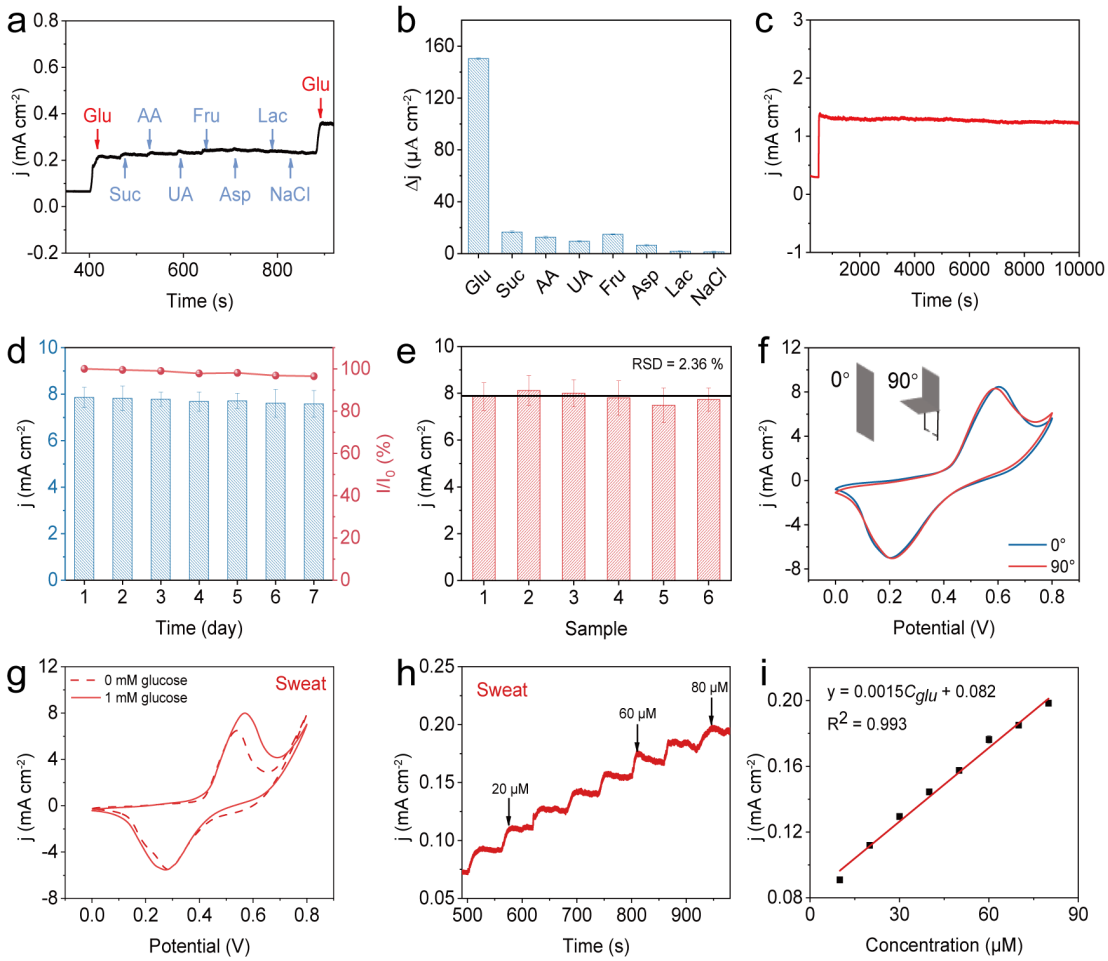

Fig. 4. (a) Amperometric responses of Ni/GF with continuous addition of glucose (1 mM) and other interfering substances (0.1 mM). (b) Comparison of changes in current density response to glucose and different interfering substances. (c) Amperometric response of Ni/GF to glucose over a long running time of 10000 s. (d) Change in current density of the same Ni/GF after repeated experiments. (e) Response current density of six parallel electrodes. (f) CV curves of Ni/GF initially and after bending at 90°. (g) CV diagram of Ni/GF in artificial sweat with or without glucose. (h) Amperometric responses of the Ni/GF to the addition of 10 μM artificial sweat. (i) Corresponding calibration curve of current density vs. glucose concentration.

To comprehensively evaluate the applicability of the Ni/GF electrode in real-world

analysis, we employed it for the detection of glucose in both artificial sweat and tea. The CVs of the prepared electrode were recorded under two conditions: with and without the addition of artificial sweat (Fig. 4g) and tea samples (Fig. S13) respectively. An evident increase in the oxidation current density was observe upon introducing glucose into the artificial sweat and tea electrolytes, confirming the analytical capability of the Ni/GF electrode for detecting glucose in practical samples. Additionally, 40 μL of 10 mM artificial sweat samples (Fig. 4h) and tea (Fig. S14) were continuously added to 40 mL of 0.1 M NaOH solution. Significantly, a rapid and sensitive response was obtained for each sample injection, demonstrating the utility of the prepared Ni/GF sensor in real-world sample analysis. Meanwhile, the glucose concentration shows a linear variation within the e of 10 μM to 80 μM respect to the current density on the Ni/GF, as illustrated in Fig. 4i and Fig. S15. The obtained linear regression equations can be represented as:

Sample (artificial sweat): j (mA cm^{-2}) = 0.0015C_{glu} (μM) + 0.082 (R^2 = 0.993)

Sample (tea): j (mA cm^{-2}) = 0.0015C_{glu} (μM) + 0.081 (R^2 = 0.993)

Subsequently, three parallel tests were conducted to assess recovery. According to the results in Table S2, the recovery rates of the spiked samples ranged from 92.60% to 105.20%, indicating that the Ni/GF electrode demonstrates good feasibility for measuring glucose in practical testing.

4. Conclusions

In summary, the Ni/GF was prepared and implemented to significantly enhance

electrochemical sensing performance for enzyme-free detection of glucose. The large wrinkling, layered multi-channel structure, and high conductivity (2.58×10^4 S m^{-1}) of GF contribute to a large specific surface area and significant electron transfer rate, facilitating the electrodeposition of nickel and the electrochemical oxidation of glucose. As a result, the customized Ni/GF electrode is endowed with a larger electrochemical active area, a remarkable charge transfer rate, and superior ion diffusivity during the glucose sensing process. Consequently, the Ni/GF electrode exhibits outstanding catalytic activity towards glucose, showcasing excellent flexibility, high sensitivity (1719.4 μA mM^{-1} cm^{-2}), rapid response time (3 s), low LOD (0.2 μM), and promising anti-interference ability. Furthermore, the prepared electrode demonstrates the ability to precisely monitor glucose concentration in artificial sweat and tea, showcasing its practical utility in real-world sample analysis. The improved electrochemical electrode platform presented in this study may provide valuable insights for the development of flexible electrode substrate materials in electrochemical analysis and sensing.

Acknowledgements

This work was supported by the National Natural Science Foundation of China (22279097, 22102128), the Key R&D Program of Hubei Province (2023BAB103), the China Postdoctoral Science Foundation (2023M732723) and the Fundamental Research Funds for the Central Universities (WUT: 2022IVA172).

References

[1] D. Won, J. Bang, S.H. Choi, K.R. Pyun, S. Jeong, Y. Lee, S.H. Ko, Transparent electronics for wearable electronics application, Chem. Rev. 123 (2023) 9982–10078, https://doi.org/10.1021/acs.chemrev.3c00139.

[2] G. Lee, M. Zarei, Q. Wei, Y. Zhu, S.G. Lee, Surface wrinkling for flexible and stretchable sensors, Small. 18 (2022) 2203491, https://doi.org/10.1002/smll.202203491.

[3] A.D. Ambaye, K.K. Kefeni, S.B. Mishra, E.N. Nxumalo, B. Ntsendwana, Recent developments in nanotechnology-based printing electrode systems for electrochemical sensors, Talanta. 225 (2021) 121951, https://doi.org/10.1016/j.talanta.2020.121951.

[4] M. Li, X. Wang, Y. Zhu, X. Jia, S. Zhang, H. Wang, Y. Li, G. Hu, Fe_2O_3-decorated boron/nitrogen-co-doped carbon nanosheets as an electrochemical sensing platform for ultrasensitive determination of paraquat in natural water, Chinese Chem. Lett. 34 (2023) 107299, https://doi.org/10.1016/j.cclet.2022.03.022.

[5] Z. Luo, X. Han, Z. Ma, B. Zhang, X. Zheng, Y. Liu, M. Gao, G. Zhao, Y. Lin, H. Pan, W. Sun, Unraveling the unique strong metal-support interaction in titanium dioxide supported platinum clusters for the hydrogen evolution reaction, Angew. Chem. Int. Ed. (2024) e202406728. https://doi.org/10.1002/anie.202406728.

[6] L. Sun, H. Guo, X. Wei, Z. Lu, M. Wang, Z. Yang, Y. Hui, Z. Yu, W. Yang, Highly crystalline polyimide covalent organic framework as electrochemical sensing

platform for the ultrasensitive detection of purine bases in DNA, Talanta. 269 (2024) 125493, https://doi.org/10.1016/j.talanta.2023.125493.

[7] X. Zheng, J. Yang, P. Li, Q. Wang, J. Wu, E. Zhang, S. Chen, Z. Zhuang, W. Lai, S. Dou, W. Sun, D. Wang, Y. Li, Ir-Sn pair-site triggers key oxygen radical intermediate for efficient acidic water oxidation, Sci. Adv. 9 (2023) eadi8025. https://doi.org/10.1126/SCIADV.ADI8025.

[8] M. Waqas, L. Yang, Y. Wei, Y. Sun, F. Yang, Y. Fan, W. Chen, Controlled fabrication of nickel and cerium mixed nano-oxides supported on carbon nanotubes for glucose monitoring, Electrochim. Acta. 440 (2023) 141735, https://doi.org/10.1016/j.electacta.2022.141735.

[9] L. Wang, H. Yu, Q. Zhang, Y. Li, W. Jia, C. Hou, H. Wang, NiCo–$NiCoO_2$/carbon hollow nanocages for non-enzyme glucose detection, Electrochim. Acta. 381 (2021) 138259, https://doi.org/10.1016/j.electacta.2021.138259.

[10] D. Chu, F. Li, X. Song, H. Ma, L. Tan, H. Pang, X. Wang, D. Guo, B. Xiao, A novel dual-tasking hollow cube $NiFe_2O_4$-NiCo-LDH@rGO hierarchical material for high preformance supercapacitor and glucose sensor, J. Colloid Interface Sci. 568 (2020) 130–138, https://doi.org/10.1016/j.jcis.2020.02.012.

[11] G. Ebrahimi, P.S. Pakchin, A. Mota, H. Omidian, Y. Omidi, Electrochemical microfluidic paper-based analytical devices for cancer biomarker detection: From 2D to 3D sensing systems, Talanta. 257 (2023) 124370, https://doi.org/10.1016/j.talanta.2023.124370.

[12] Z. Li, Y. Chen, T. Ma, Y. Jiang, J. Chen, H. Pan, W. Sun, 2D metal-free nanomaterials beyond graphene and its analogues toward electrocatalysis applications, Adv. Energy Mater. 11 (2021) 2101202. https://doi.org/10.1002/aenm.202101202.

[13] Á. Torrinha, S. Morais, Electrochemical (bio) sensors based on carbon cloth and carbon paper: An overview, Trac-Trends Anal. Chem. 142 (2021) 116324, https://doi.org/10.1016/j.trac.2021.116324.

[14] Y. Chen, B. Zhang, Y. Liu, J. Chen, H. Pan, W. Sun, Graphitic carbon nitride-based electrocatalysts for energy applications, Mater. Today Catal. 1 (2023) 100003. https://doi.org/10.1016/j.mtcata.2023.100003.

[15] M. Şen, M. Oğuz, İ. Avcı, Non-toxic flexible screen-printed MWCNT-based electrodes for non-invasive biomedical applications, Talanta. 268 (2024) 125341, https://doi.org/10.1016/j.talanta.2023.125341.

[16] M. Ni, M. Tan, Y. Pan, C. Zhu, H. Du, Rapid preparation of self-supported nickel-iron oxide as a high-performance glucose sensing platform, J. Mater. Chem. C. 10 (2022) 12883–12891, https://doi.org/10.1039/d2tc03176k.

[17] S. Guo, H. Shen, Z. Tie, S. Zhu, P. Shi, J. Fan, Q. Xu, Y. Min, Three-dimensional cross-linked polyaniline fiber/n-doped porous carbon with enhanced electrochemical performance for high-performance supercapacitor, J. Power Sources. 359 (2017) 285–294, https://doi.org/10.1016/j.jpowsour.2017.04.100.

[18] Q. Zhang, Y. He, G. Lin, X. Ma, Z. Xiao, D. Shi, Y. Yang, In situ growth of

polyimide nanoarrays on conductive carbon supports for high-rate charge storage and long-lived metal-free cathodes, J. Mater. Chem. A. 9 (2021) 10652–10660, https://doi.org/10.1039/d1ta00302j.

[19] D. Zhao, R. Zhao, S. Dong, X. Miao, Z. Zhang, C. Wang, L. Yin, Alkali-induced 3D crinkled porous Ti_3C_2 MXene architectures coupled with NiCoP bimetallic phosphide nanoparticles as anodes for high-performance sodium-ion batteries, Energy Environ. Sci. 12 (2019) 2422–2432, https://doi.org/10.1039/c9ee00308h.

[20] Z. Yin, S. He, Y. Li, W. Dai, H. Wang, R. He, K. Tang, Y. Xiao, S. Wang, J. Gao, L. Zhang, J. Li, N. Tang, Z. Yin, Self-supported carbon electrodes with a carbon membrane and Co_3O_4 nanosheets for high-performance enzymeless glucose detection and supercapacitors, ACS Appl. Nano Mater. 6 (2023) 6208–6220, https://doi.org/10.1021/acsanm.3c00505.

[21] J.M. Mohan, K. Amreen, A. Javed, S.K. Dubey, S. Goel, Miniaturized 3D printed electrochemical platform with optimized fibrous carbon electrode for non-interfering hypochlorite sensing, Chemosphere. 302 (2022) 134915, https://doi.org/10.1016/j.chemosphere.2022.134915.

[22] A. Farid, C. Zhonghua, A.S. Khan, M. Javid, I.A. Khan, A.A. Khan, Z. Fan, L. Pan, $Ni_3V_2O_8$ nanosheets grafted on 3D helical-shaped carbon nanocoils as a binder-free hierarchical composite for efficient non-enzymatic glucose sensing, Adv. Funct. Mater. 33 (2023) 2301727, https://doi.org/10.1002/adfm.202301727.

[23] L. Yan, P. Ma, Y. Liu, X. Ma, F. Chen, M. Li, 3D coral-like gold/carbon paper

electrode modified with covalent and cross-linked enzyme aggregates for electrochemical sensing of glucose, Microchem. J. 159 (2020) 105347, https://doi.org/10.1016/j.microc.2020.105347.

[24] K.Y. Lau, J. Qiu, Broad applications of sensors based on laser-scribed graphene, Light Sci. Appl. 12 (2023) 168, https://doi.org/10.1038/s41377-023-01210-6.

[25] J. Wu, H. Lin, D.J. Moss, K.P. Loh, B. Jia, Graphene oxide for photonics, electronics and optoelectronics, Nat. Rev. Chem. 7 (2023) 162–183, https://doi.org/10.1038/s41570-022-00458-7.

[26] A. Ahmed, A. Singh, S.J. Young, V. Gupta, M. Singh, S. Arya, Synthesis techniques and advances in sensing applications of reduced graphene oxide (rGO) composites: A review, Compos. Part A Appl. Sci. Manuf. 165 (2023) 107373, https://doi.org/10.1016/j.compositesa.2022.107373.

[27] Y. Luo, B. Zhu, S. Zhang, P. Zhang, X. Li, L. Wang, B. Lu, J. Travas-Sejdic, Stretchable and flexible non-enzymatic glucose sensor based on poly (ether sulfone)-derived laser-induced graphene for wearable skin diagnostics, Adv. Mater. Technol. 7 (2022) 2101571, https://doi.org/10.1002/admt.202101571.

[28] T.D. Le, H. Phan, S. Kwon, S. Park, Y. Jung, J. Min, B.J. Chun, H. Yoon, S.H. Ko, S. Kim, Y. Kim, Recent advances in laser-induced graphene : Mechanism , fabrication , properties , and applications in flexible electronics, Adv. Funct. Mater. 32 (2022) 2205158, https://doi.org/10.1002/adfm.202205158.

[29] L. Peng, Y. Han, M. Wang, X. Cao, J. Gao, Y. Liu, X. Chen, B. Wang, B. Wang,

C. Zhu, X. Wang, K. Cao, M. Huang, B. V. Cunning, J. Pang, W. Xu, Y. Ying, Z. Xu, W. Fang, Y. Lu, R.S. Ruoff, C. Gao, Multifunctional macroassembled graphene nanofilms with high crystallinity, Adv. Mater. 33 (2021) 2104195. https://doi.org/10.1002/adma.202104195.

[30] Y. Liu, M. Zhang, Q. Huang, X. Wang, P. Xu, X. Lin, W. Song, K.X. Ba, Vertical graphene on graphene composite film for heat dissipation and electromagnetic shielding, ACS Appl. Nano Mater. 7 (2024) 5074–5084. https://doi.org/10.1021/acsanm.3c05864.

[31] K. Shen, P. Li, J. Lin, Z. Wang, G. Cai, X. Ming, Y. Liu, C. Gao, Z. Xu, Intercalated oligomer doubles plasticity for strong and conductive graphene papers and composites, Carbon 208 (2023) 160–169, https://doi.org/10.1016/j.carbon.2023.03.036.

[32] R. Song, B. Mao, Z. Wang, Y. Hui, N. Zhang, R. Fang, J. Zhang, Y. Wu, Q. Ge, K. Novoselovb, D. He, Comparison of copper and graphene-assembled films in 5G wireless communication and THz electromagnetic-interference shielding, Proc. Natl. Acad. Sci. 120 (2023) e2209807120, https://doi.org/10.1073/pnas.2209807120.

[33] T. Sun, L. Shen, Y. Jiang, J. Ma, F. Lv, H. Ma, D. Chen, N. Zhu, Wearable textile supercapacitors for self-powered enzyme-free smartsensors, ACS Appl. Mater. Interfaces. 12 (2020) 21779–21787, https://doi.org/10.1021/acsami.0c05465.

[34] X. Wang, J. Zhou, W. Cui, F. Gao, Y. Gao, F. Qi, Y. Liu, X. Yang, K. Wang, Z.

Li, Y. Yang, J. Chen, W. Sun, L. Sun, H. Pan, Electron manipulation and surface reconstruction of bimetallic iron–nickel phosphide nanotubes for enhanced alkaline water electrolysis, Adv. Sci. 11 (2024) 2401207. https://doi.org/10.1002/advs.202401207.

[35] M. Lu, Y. Deng, Y. Li, T. Li, J. Xu, S.W. Chen, J. Wang, Core-shell MOF@MOF composites for sensitive nonenzymatic glucose sensing in human serum, Anal. Chim. Acta. 1110 (2020) 35–43, https://doi.org/10.1016/j.aca.2020.02.023.

[36] Y. Zhang, Y.Q. Liu, Y. Bai, W. Chu, J. Sh, Confinement preparation of hierarchical NiO-n-doped carbon@reduced graphene oxide microspheres for high-performance non-enzymatic detection of glucose, Sensors Actuators, B Chem. 309 (2020) 127779, https://doi.org/10.1016/j.snb.2020.127779.

[37] Y. zhang, P. Xia, H. Fan, X. Gao, F. Ouyang, W. Chen, In-situ growth of CoO nanoneedles array on 3D nickel foam toward high-performance glucose sensor, Dalt. Trans. 52 (2023) 2603-2610, https://doi.org/10.1039/d2dt03877c.

[38] Z. Xu, Q. Wang, H. Zhangsun, S. Zhao, Y. Zhao, L. Wang, Carbon cloth-supported nanorod-like conductive Ni/Co bimetal MOF: A stable and high-performance enzyme-free electrochemical sensor for determination of glucose in serum and beverage, Food Chem. 349 (2021) 129202, https://doi.org/10.1016/j.foodchem.2021.129202.

[39] B. Long, P. Cao, Y. Zhao, Q. Fu, Y. Mo, Y. Zhai, J. Liu, Pt_1/Ni_6Co_1 layered double hydroxides/n-doped graphene for electrochemical non-enzymatic glucose sensing

by synergistic enhancement of single atoms and doping, Nano Res. 16 (2022) 318–324, https://doi.org/10.1007/s12274-022-4801-9.

[40] Y. Zhao, Y. Jiang, Y. Mo, Y. Zhai, J. Liu, A.C. Strzelecki, X. Guo, C. Shan, Boosting electrochemical catalysis and nonenzymatic sensing toward glucose by single-atom Pt supported on Cu@CuO core–shell nanowires, Small. 19 (2023) 2207240, https://doi.org/10.1002/smll.202207240.

[41] Q. Wang, K. Chen, H. Jiang, C. Chen, C. Xiong, M. Chen, J. Xu, X. Gao, S. Xu, H. Zhou, Y. Wu, Cell-inspired design of cascade catalysis system by 3D spatially separated active sites, Nat. Commun. 14 (2023) 5338, https://doi.org/10.1038/s41467-023-41002-5.

[42] H. Wang, W. Zhu, T. Xu, Y. Zhang, Y. Tian, X. Liu, J. Wang, M. Ma, An integrated nanoflower-like MoS_2@$CuCo_2O_4$ heterostructure for boosting electrochemical glucose sensing in beverage, Food Chem. 396 (2022) 133630, https://doi.org/10.1016/j.foodchem.2022.133630.

Supplementary Material

Flexible, scalable hierarchical graphene foam decorated with nickel layer for highly sensitive enzyme-free glucose sensing

Xiaodong Ji [a,b], Huihui Jin [c,d,*], Wei Qian [d], Zhe Wang [e], Zixin Zhang [b], Zhugen Yang [f], Daping He [a,b,d,*]

[a] Sanya Science and Education Innovation Park of Wuhan University of Technology, Sanya 572000, China

[b] School of Materials Science and Engineering, Wuhan University of Technology, Wuhan 430070, China

[c] School of Science, Wuhan University of Technology, Wuhan 430070, China

[d] Hubei Engineering Research Center of RF-Microwave Technology and Application, Wuhan University of Technology, Wuhan 430070, China

[e] State Key Laboratory of Advanced Technology for Materials Synthesis and Processing, Wuhan University of Technology, Wuhan 430070, China

[f] School of Water, Energy and Environment, Cranfield University, Cranfield, MK43 0AL, United Kingdom

[*]Corresponding author.

Email-address: jinhuihui@whut.edu.cn (Huihui Jin), hedaping@whut.edu.cn (Daping He)

Materials characterization

The sample morphologies and microstructures were analyzed using a filed-emission scanning electron microscopy (FESEM, JSM-7610F Plus) at an accelerating voltage of 5.0-15.0 kV. The sample morphologies and roughness were observed by a white light interferometer (NewView 7100). Electronic structure and the components of samples were characterized with X-ray photoelectron spectroscopy (XPS, CoreTech Int, PHI VersaProbe 4) by Al-Kα radiation. Raman spectrum was collected by RENISHAW with a laser wavelength of 532 nm. The crystal information measurements were collected with X-ray diffraction (XRD, Rigaku Smartlab) using Cu Kα (λ=1.5406 Å) radiation. The hydrophilicity and hydrophobicity of the samples were characterized using an optical water contact angle meter (Biolin Scientific Theta lite). The adhesion of samples was tested on a universal testing machine (MTS E44.104). The electrical conductivity of the samples was characterized by a standard four-probe technique (ROOKO, RK-YA).

Adsorption of glucose on the Ni/GF electrode surface calculation

The glucose adsorbed on the Ni/GF electrode surface can be quantified by following Brown-Anson model:

$$I_p = nFAQv/4RT = n^2F^2A\nu\Gamma/4RT$$

Where n is the electron transfer number (n = 1), A is the surface area of electrode (A

= 1 cm^2), Q is the amount of charge consumed by the electrooxidation reaction (Q = nFAΓ), ν is the scan rate (ν = 0.05 v/s), F is the Faraday constant (F = 96485 mol/C), R is the gas constant (R = 8.314 J/mol), and T is the temperature (T = 298 K).

Electrocatalytic oxidation mechanism of the Ni/GF electrode

The mechanism of glucose electrochemical oxidation relies on a nickel-based electrocatalyst. In this process, Ni is first oxidized to $Ni(OH)_2$ (Equation (1)), and $Ni(OH)_2$ is further oxidized to NiOOH (Equation (2)). Upon the addition of glucose, NiOOH oxidizes glucose to gluconolactone while simultaneously regenerating $Ni(OH)_2$ (Equation (3)). The following equations represent the electrocatalytic oxidation mechanism of the electrode:

$$Ni + 2OH^- \rightarrow Ni(OH)_2 + 2e^- \quad (1)$$

$$Ni(OH)_2 + OH^- \rightarrow NiOOH + H_2O + e^- \quad (2)$$

$$2NiOOH + Glucose \rightarrow Gluconolactone + 2Ni(OH)_2 \quad (3)$$

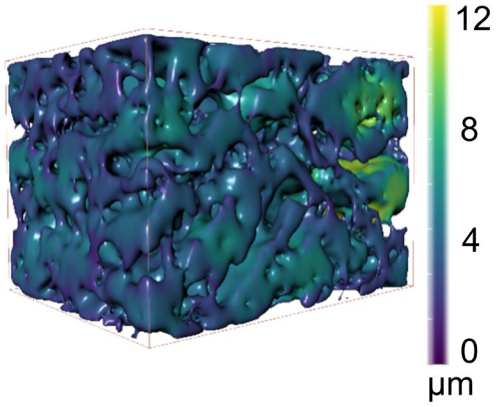

Fig. S1. Three-dimensional CT image of GF.

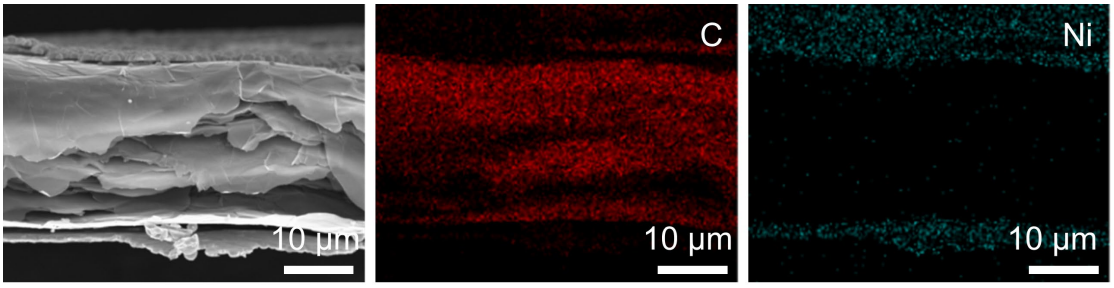

Fig. S2. Cross-sectional morphology of Ni/cGF and corresponding EDS mapping.

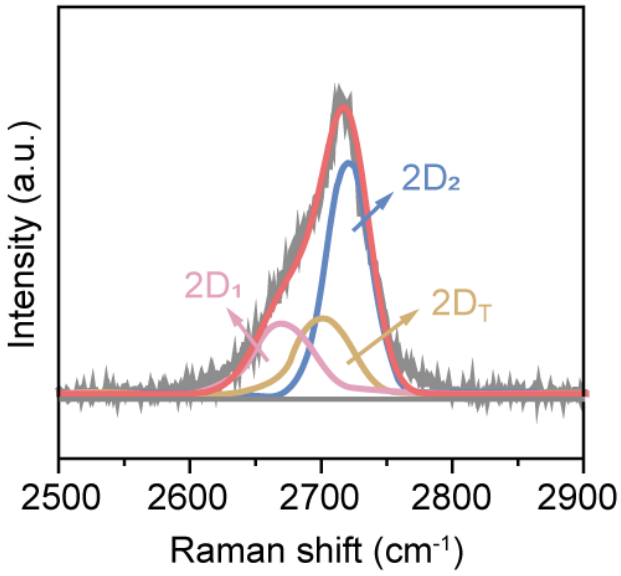

Fig. S3. Fitted 2D peak of Raman spectrum.

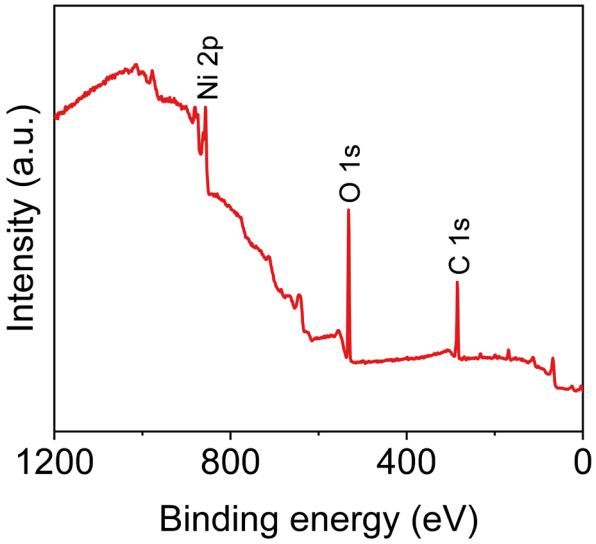

Fig. S4. XPS full spectra of Ni/GF.

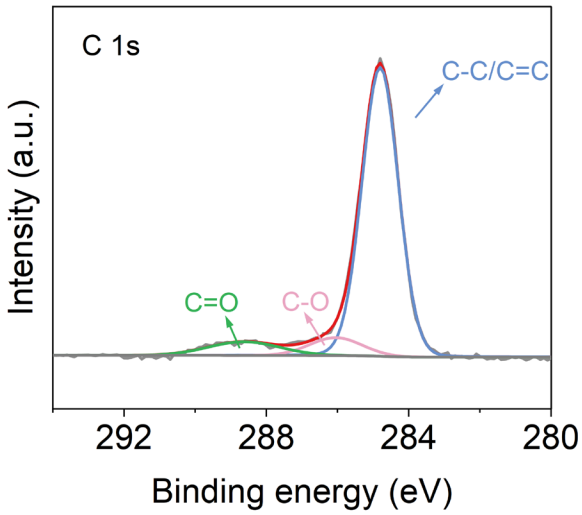

Fig. S5. XPS C 1s spectra of Ni/GF.

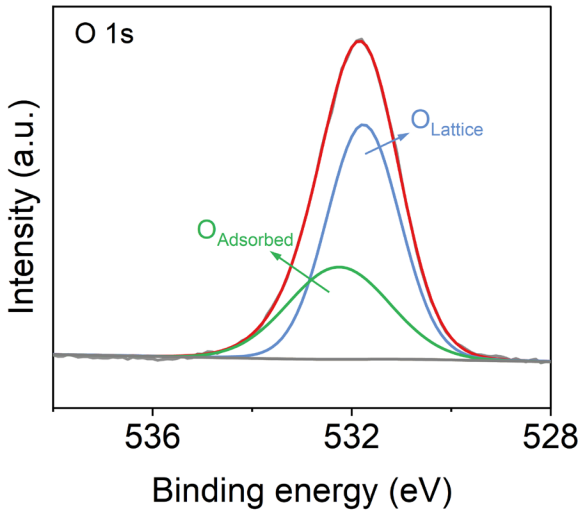

Fig. S6. XPS O 1s spectra of Ni/GF.

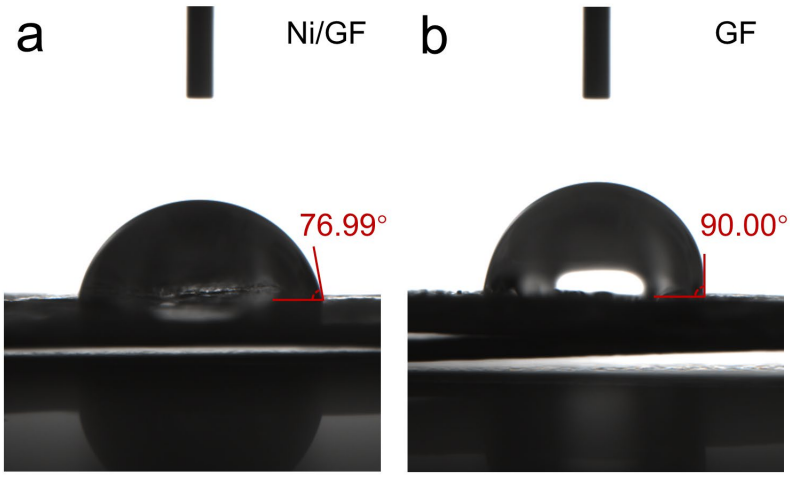

Fig. S7. Water contact angle of the Ni/GF (a) and GF (b).

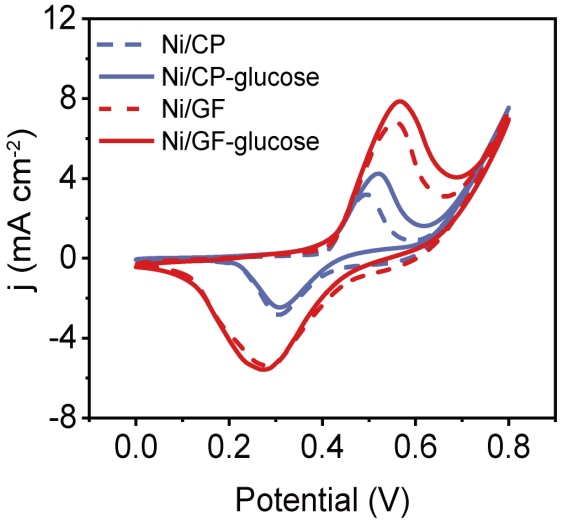

Fig. S8. CV diagram of Ni/CP, and Ni/GF under the condition of absence or presence glucose.

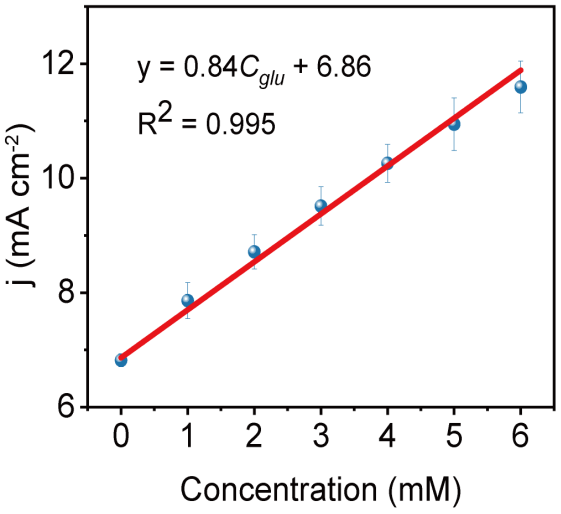

Fig. S9. The corresponding calibration curve of current density and glucose concentration ranging from 0 mM to 6 mM.

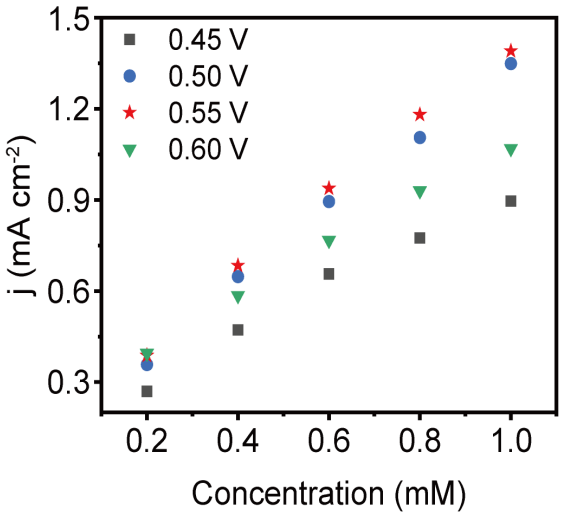

Fig. S10. The scatter diagram of optimum potential for the Ni/GF at different potentials (0.45-0.60 V).

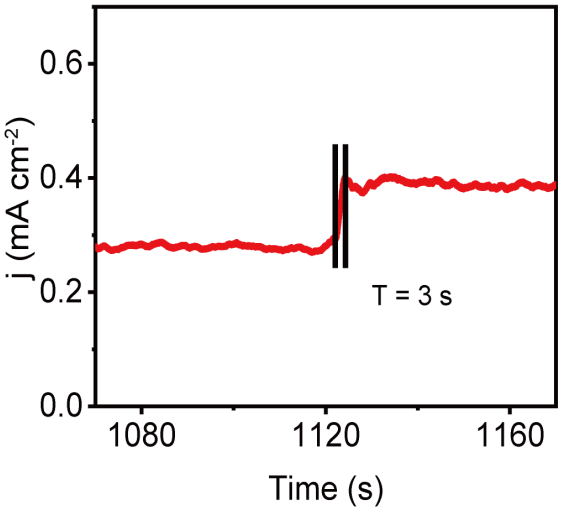

Fig. S11. Response time of the Ni/GF.

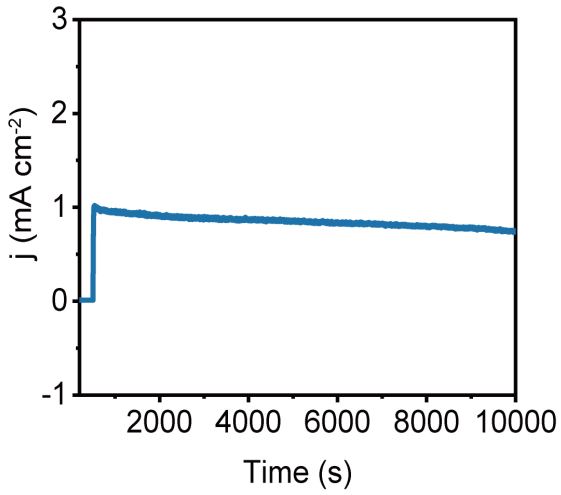

Fig. S12. Ampermetric response of the Ni/cGF for glucose over a long running time of 10000 s.

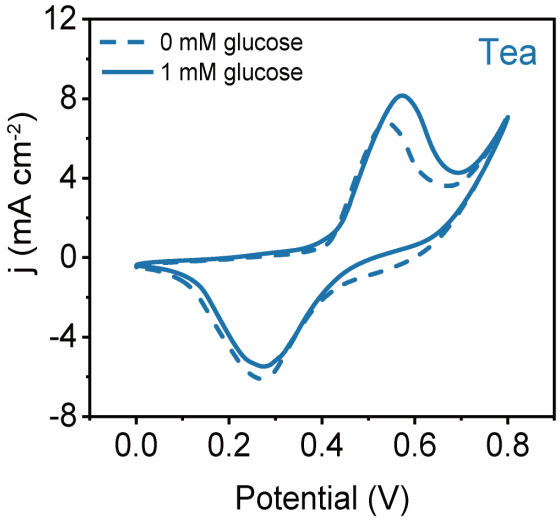

Fig. S13. CV diagram of Ni/GF in tea under the condition of absence or presence glucose.

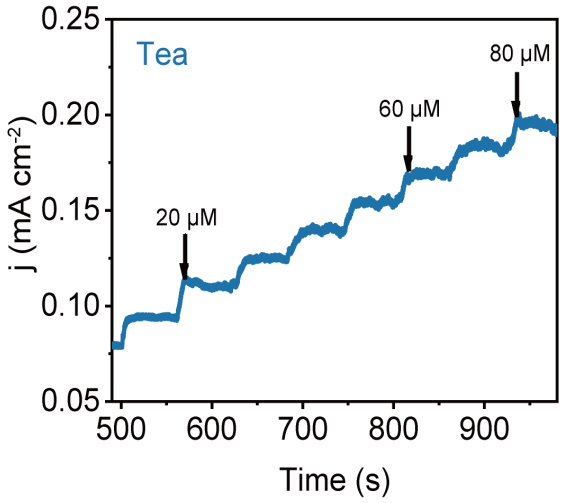

Fig. S14. Amperometric responses of the Ni/GF to the addition of 10 μM tea.

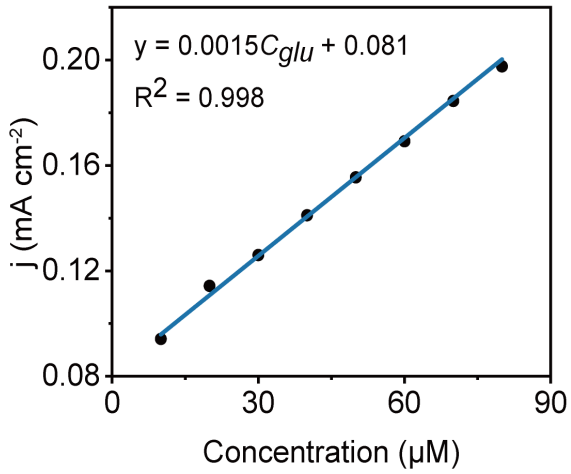

Fig. S15. The corresponding linear calibration curve of current density versus glucose concentration.

Table S1 Comparison of analytical performance of different electrode materials for glucose detection.

Electrode materials	Liner range (mM)	Sensitivity ($\mu A\ mM^{-1}\ cm^{-2}$)	LOD (μM)	Response time (s)	Ref
NiSA/NC/GCE	0.0008-1.124	799.43	0.22	-	[1]
MoS_2@$CuCo_2O_4$/GCE	0.0005-0.393	1303	0.5	2.1	[2]
Co-Ni(Fe)-MOF/PPy/GCE	0.002-3	1805	1.13	-	[3]
Pt_1/Cu@CuO/GCE	0.00001-0.00518	852.163	3.6	-	[4]
NiO-NPs-GCE	0.05-1 1-10	791 198	6.4	2.8	[5]
Au@Ni-Fe PBA/Nifion	0.01-16	8.037	4.686	-	[6]
α-CD-rGO/Ni-MOF/TM	0.00065-4.828 4.828-9.178	1395 760	0.3	1.9	[7]
3D MgO/CC	0.04-6.85	198	0.41	10	[8]
Au NFs@CC	0.005-4	63.9	5.18	2.3	[9]
Ni(OH)/F@GF	0.01-7.66	595.3	1	3	[10]
Cu_2O-Au-LIG	1-20	236	0.31	<15	[11]
Co_3O_4 NPs-LIG	0.001-9	214	0.41	0.49	[12]
AgNPs@NiCo-MOF/SPE	0.005-1.125 1.525-5.325	1191.84 271.19	2.3	4	[13]
Ni/GF	0.0005-1	1719.38	0.2	3	This work

Table S2 Detection of glucose in artificial sweat and tea samples using the Ni/GF.

Samples	Added (μM)	Detected (μM)	Recovery (%)	RSD (%)
Artificial sweat	5.00	5.26	105.20	2.19
	10.00	9.97	99.70	1.59
	15.00	15.23	101.53	2.55
Tea	5.00	5.03	100.60	2.95
	10.00	9.26	92.60	5.37
	15.00	15.40	102.67	3.98

References

[1] H. Yin, X. Bai, Z. Yang, Activating Ni nanoparticles into Ni single atoms by n doping for high-performance electrochemical sensing of glucose, Chem. Eng. J. 478 (2023) 147510, https://doi.org/10.1016/j.cej.2023.147510.

[2] H. Wang, W. Zhu, T. Xu, Y. Zhang, Y. Tian, X. Liu, J. Wang, M. Ma, An integrated nanoflower-like MoS_2@$CuCo_2O_4$ heterostructure for boosting electrochemical glucose sensing in beverage, Food Chem. 396 (2022) 133630, https://doi.org/10.1016/j.foodchem.2022.133630.

[3] S. Chen, D. Liu, N. Song, C. Wang, X. Lu, Promoting non-enzymatic electrochemical sensing performance toward glucose by the integration of conducting polypyrrole with metal-organic framework, Compos. Commun. 30 (2022) 101074, https://doi.org/10.1016/j.coco.2022.101074.

[4] Y. Zhao, Y. Jiang, Y. Mo, Y. Zhai, J. Liu, A.C. Strzelecki, X. Guo, C. Shan, Boosting electrochemical catalysis and nonenzymatic sensing toward glucose by single-atom Pt supported on Cu@CuO core–shell nanowires, Small. 19 (2023) 2207240, https://doi.org/10.1002/smll.202207240.

[5] M. Youcef, B. Hamza, H. Nora, B. Walid, M. Salima, B. Ahmed, F. Malika, S. Marc, B. Christian, D. Wassila, M. Djamel Eddine, Z. Larbi, A novel green synthesized NiO nanoparticles modified glassy carbon electrode for non-enzymatic glucose sensing, Microchem. J. 178 (2022) 107332, https://doi.org/10.1016/j.microc.2022.107332.

[6] L. Shen, Z. Liang, Z. Chen, C. Wu, X. Hu, J. Zhang, Q. Jiang, Y. Wang, Reusable electrochemical non-enzymatic glucose sensors based on Au-inlaid nanocages, Nano Res. 15 (2022) 6490-6499, https://doi.org/10.1007/s12274-022-4219-4.

[7] T. Xu, Y. Zhang, M. Liu, H. Wang, J. Ren, Y. Tian, X. Liu, Y. Zhou, J. Wang, W. Zhu, M. Ma, In-situ two-step electrodeposition of α-CD-rGO/Ni-MOF composite film for superior glucose sensing, J. Alloys Compd. 923 (2022) 166418, https://doi.org/10.1016/j.jallcom.2022.166418.

[8] M. Hilal, J. In Han, Facile preparation of three-dimensional hierarchical MgO microstructures for non-enzymatic glucose sensor, Appl. Surf. Sci. 619 (2023) 156750, https://doi.org/10.1016/j.apsusc.2023.156750.

[9] Z. Zhao, T. Wang, K. Li, D. Long, J. Zhao, F. Zhu, W. Gong, A flexible nonenzymatic sweat glucose sensor based on Au nanoflowers coated carbon cloth, Sensors Actuators B Chem. 388 (2023) 133798, https://doi.org/10.1016/j.snb.2023.133798.

[10] Z. Zhu, Y. Wu, J. Yang, Y. Xue, Core-sheath fibers composed of f-doped nickel hydroxide nanorods and graphene fibers for effective fiber-shaped nonenzymatic glucose sensors, J. Alloys Compd. 889 (2022) 161608, https://doi.org/10.1016/j.jallcom.2021.161608.

[11] Y. Huang, Y. Han, J. Sun, Y. Zhang, L. Han, Dual nanocatalysts co-decorated three-dimensional, laser-induced graphene hybrid nanomaterials integrated with a smartphone portable electrochemical system for point-of-care non-enzymatic

glucose diagnosis, Mater. Today Chem. 24 (2022) 100895, https://doi.org/10.1016/j.mtchem.2022.100895.

[12] J. Zhao, C. Zheng, J. Gao, J. Gui, L. Deng, Y. Wang, R. Xu, Co_3O_4 nanoparticles embedded in laser-induced graphene for a flexible and highly sensitive enzyme-free glucose biosensor, Sensors Actuators B Chem. 347 (2021) 130653, https://doi.org/10.1016/j.snb.2021.130653.

[13] Y. Ma, Y. Leng, D. Huo, D. Zhao, J. Zheng, P. Zhao, H. Yang, F. Li, C. Hou, A portable sensor for glucose detection in huangshui based on blossom-shaped bimetallic organic framework loaded with silver nanoparticles combined with machine learning, Food Chem. 429 (2023) 136850, https://doi.org/10.1016/j.foodchem.2023.136850.

https://dspace.org/

Flexible, scalable hierarchical graphene foam decorated with nickel layer for highly sensitive enzyme-free glucose sensing

Ji, Xiaodong; Jin, Huihui; Qian, Wei; Wang, Zhe; Zhang, Zixin ...

2024-11-05
Elsevier
https://doi.org/10.1016/j.jallcom.2024.175902
Ji X, Jin H, Qian W, et al., (2024) Flexible, scalable hierarchical graphene foam decorated with nickel layer for highly sensitive enzyme-free glucose sensing. Journal of Alloys and Compounds, Volume 1004, November 2024, Article number 175902

Downloaded from a DSpace repository. https://dspace.org/